Ion beam induced charge microscopy studies of power diodes

2004 J. Phys.: Condens. Matter 16 S57

(http://iopscience.iop.org/0953-8984/16/2/007)

INSTITUTE OF PHYSICS PUBLISHING JOURNAL OF PHYSICS: CONDENSED MATTER

J. Phys.: Condens. Matter **16** (2004) S57–S66 PII: S0953-8984(04)66917-7

Ion beam induced charge microscopy studies of power diodes

M Zmeck[1,2,3], L J Balk[1], T Osipowicz[2], F Watt[2], J C H Phang[3], A M Khambadkone[4], F-J Niedernostheide[5] and H-J Schulze[5]

[1] Fachbereich Elektrotechnik & Informationstechnik, Lehrstuhl für Elektronik, Bergische Universität Wuppertal, Rainer-Gruenter-Straße 21, D-42119 Wuppertal, Germany
[2] Centre for Ion Beam Applications, Department of Physics, National University of Singapore, 2 Science Drive 3, 117542 Singapore, Singapore
[3] Centre for Integrated Circuit Failure Analysis and Reliability, Department of Electrical and Computer Engineering, National University of Singapore, 10 Kent Ridge Crescent, 119260 Singapore, Singapore
[4] Centre for Power Electronics, Department of Electrical and Computer Engineering, National University of Singapore, 4 Engineering Drive 3, 117576 Singapore, Singapore
[5] Infineon AG, AI PS DD2 TD, Balanstrasse 59, D-81541 München, Germany

Received 31 July 2003
Published 22 December 2003
Online at stacks.iop.org/JPhysCM/16/S57 (DOI: 10.1088/0953-8984/16/2/007)

Abstract

Ion beam induced charge microscopy (IBIC microscopy) has been established recently as an analytical tool for the characterization of various types of semiconductor devices. In this paper the potential of IBIC microscopy for the analysis of deeply buried structures of high power devices under biases of more than 2 kV is discussed. Such data are useful in the design process of high power devices because excessive fields at device edge regions or within protection elements (e.g. field ring structures) can be avoided.

Since charge collection efficiency within depleted pn junctions is typically 100% for IBIC analysis, the contrast due to E-field variations within the large depletion regions of high power devices is limited. Here we will introduce a new approach for enhancing this contrast by using the temporal information from the IBIC signals gained with a transient IBIC set-up. Simulations and experimental data will be compared to evaluate the suitability of the new approach. The device used here is a high voltage diode with a field ring structure which was analysed using a 2 MeV proton beam.

1. Introduction

IBIC analysis is mainly used for the analysis of integrated circuits [1] or electronic components, e.g. LEDs [2] or CMOS transistors [3], as well as for the analysis of CVD polycrystalline diamond films for radiation sensors [4].

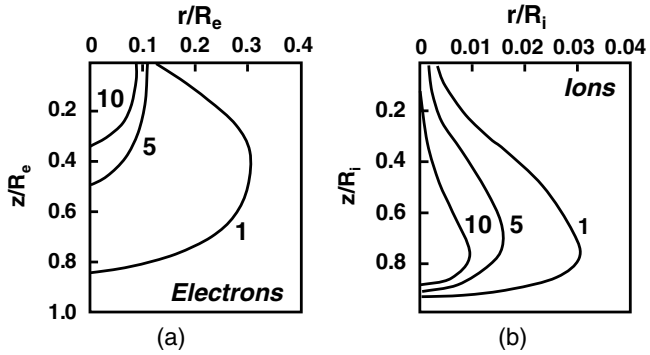

Figure 1. Generation volumes for (a) electrons and (b) protons normalized to their penetration depth.

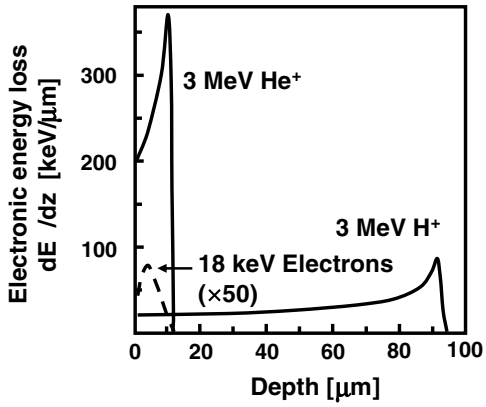

Figure 2. Electronic energy loss versus penetration depth for 3 MeV protons compared to 3 MeV He^+ ions and 18 keV electrons.

Less work can be found where IBIC analysis is applied to the analysis of the large depletion regions that are common in power devices. In this paper, the main objective is to show that electrical field distributions in such devices can be imaged by IBIC. We report the analysis of a field ring structure embedded in the large depletion region of a biased high voltage diode using IBIC microscopy. Data pertaining to the electrical field strength distribution are crucial for the design of high voltage devices and their termination structure, e.g. field ring (floating ring) termination [5].

Our previous work on high power devices (light-triggered thyristors [6] and high voltage diodes with field ring structures [7]) clearly demonstrated that IBIC is a promising tool for the analysis of deeply buried structures of high power devices.

Light ions, like 3 MeV protons, exhibit a very small lateral spread of about 6 μm in diameter when structures in a depth of more than 100 μm are analysed (figure 1). In contrast to this, electrons show a spherical generation volume. A further advantage of the use of light ions is that they lose most of their energy close to the end of the generation volume (figure 2). This reduces topographical influences and makes IBIC microscopy most sensitive to the region close to the end of the ion range. Therefore, the use of different ion energies enables also a depth resolution.

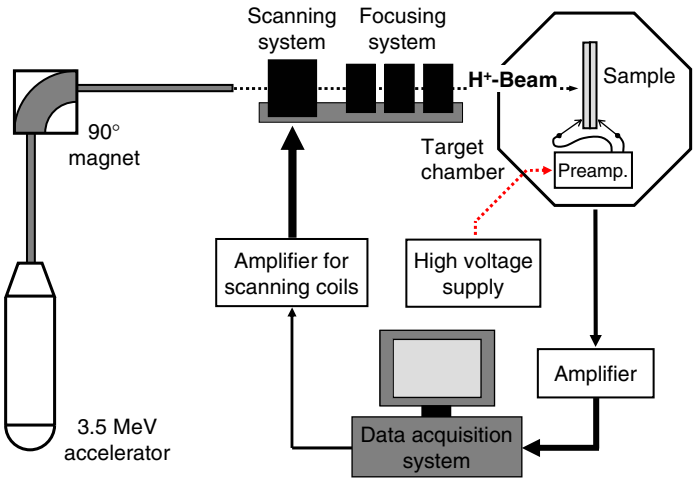

Figure 3. The IBIC set-up used for the experiments.

While penetrating into the semiconductor, each individual ion generates so many electron–hole pairs that the generated charge can be detected by a charge sensitive preamplifier. This means that each individual ion generates information, which allows a spectral analysis.

The high drift velocity of the charge carriers under the influence of the electrical field within the depletion region leads to a fast charge collection process compared to the lifetime of the charge carriers. Therefore, recombination processes within the depletion region can be neglected [8, 9].

Considering the situation in high power devices, the generation volume of the individual incident ions is almost completely embedded in the depletion region, which extends typically over a large area of the device when a high voltage is applied to the device. Therefore, the charge collection efficiency is about 100% regardless of the electrical field strength. Therefore, no significant contrast due to the electrical field variations within the depletion regions can be expected. In this paper it is shown that the temporal behaviour of IBIC signals can be used to extract information about the electric field distribution in semiconductor devices.

2. Experimental set-up

The measurements were carried out at the nuclear microprobe facility, Research Centre for Ion Beam Applications, National University of Singapore. The 2 MeV proton beam used for the experiments was generated by a 3.5 MeV singletron accelerator. The end-station OM2000 provides the microprobe focusing system consisting of a high excitation magnetic quadrupole lens triplet, prefocus scan coils for the beam scanning and an octagonal target chamber. A special target ladder has been designed which allows well organized central wiring of all connections needed for the experiment at its upper end. This ensures that the high voltage wire connected through a separated feedthrough at one of the sidewalls of the chamber is spatially separated from the sensitive wiring of the preamplifier mounted on the back of the target holder. The preamplifier used is an AmpTek A250, which is a vacuum tight miniature preamplifier. The data acquisition has been performed using the OMDAQ software package. Figure 3 shows a diagram of the experimental set-up.

The device investigated is a high voltage diode with a field ring structure consisting of seven rings (figure 4). The diode is connected to the preamplifier via the anode (top) and cathode metallization (bottom).

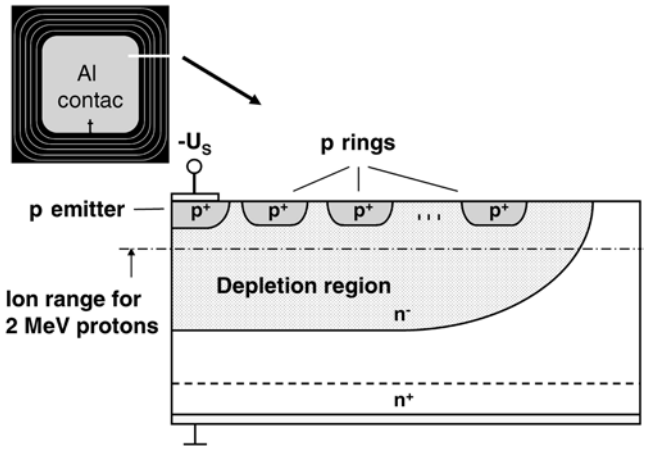

Figure 4. The cross section of the high voltage diode under investigation. Three of the seven rings are sketched; the four missing rings are indicated by three dashes.

3. Experimental results

Figure 5 shows the median value images and spectra taken for the high voltage diode for different bias voltages between 40 and 2290 V. The number of detected field rings increases with increasing bias voltage. This indicates the lateral spread of the depletion region towards the device edges with increasing bias voltage.

The homogeneous area in the bottom left corner for all four median value images corresponds to the region of the main p region which is covered by the aluminium metallization. The brighter region surrounding this area is the p region which is not covered by aluminium. The highest signals are collected at the edge of the p emitter region. The thin lines with higher intensity embedded between broader and darker lines are formed by the outer edges of the individual field rings. The appearance of higher IBIC signals at the outer edges of the field rings agrees with the appearance of maxima of the electric field distribution at these positions. This effect was clearly visible in simulations generated using the device simulation software code MEDICI. At a voltage of 2290 V a small localized bright spot in the field ring structure is visible (marked by a circular ring in the corresponding IBIC image of figure 5). This spot is caused by a defect in the device structure. The scattered appearance of individual one pixel spikes, largely in the region outside the device, is an artefact induced by the data acquisition software.

The spectra shown in the right column in figure 5 were obtained by dividing the maximum of the measurable charge collection signal into 2049 intervals subsequently labelled as channels. Each spectrum in the right column shows the total number of events calculated from the corresponding IBIC image in the left column as a function of the channel numbers. These spectra can be calibrated with respect to the collected charge or the commonly used charge collection efficiency. Each peak in the spectra represents a particular feature of the device, for example, one of the field rings, the covered or uncovered p region in the centre of the device, or the outer edges of the individual field rings. Defining a window over a certain data range in the spectra—e.g., an interval covering a single peak—enables the generation of a map reflecting the spatial distribution of one of the particular features mentioned above. In this way, we found that the peaks ‘a’ and ‘b’ in figure 5 reflect the uncovered p region and the outer edge of the first field ring, respectively. Comparing the spectra of all four bias voltages,

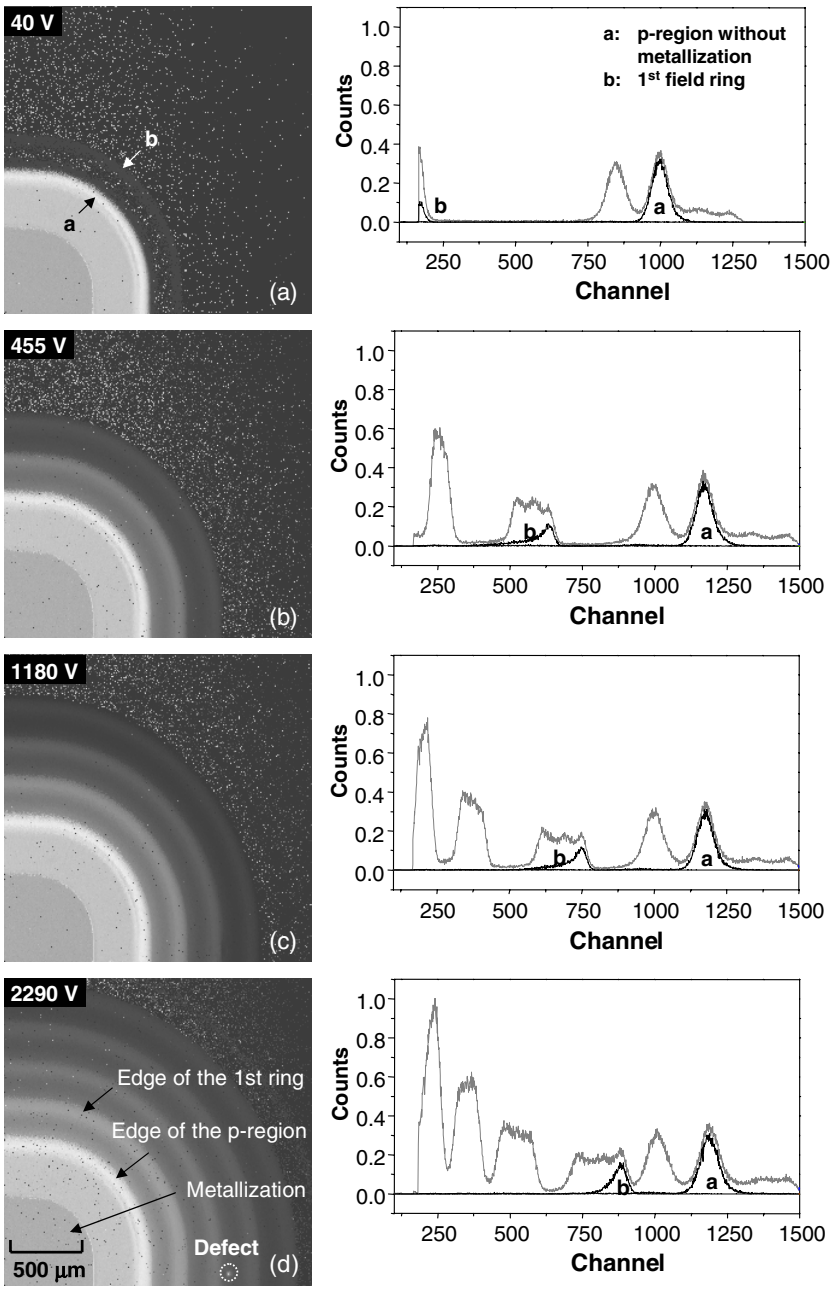

Figure 5. Median value IBIC images for different bias voltages (left) and their charge spectra (right).

peak 'a' increases only slightly when the voltage is increased from 40 to 455 V and is nearly constant for higher voltages. This means that saturation of the IBIC signal occurs when a certain field strength has been exceeded. Since the space charge region expands from the junction formed by the p emitter and the n^- region (figure 4), this happens first in the centre of the device.

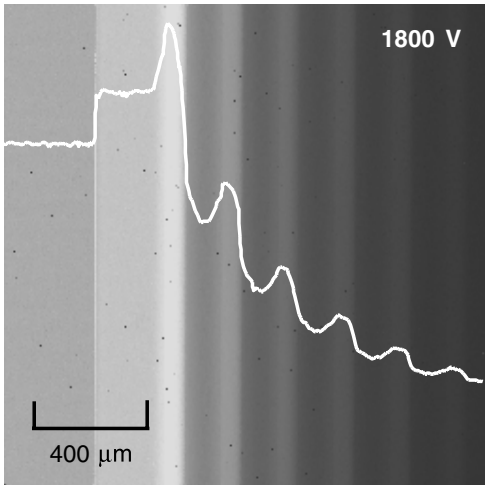

Figure 6. A median value IBIC image with a superimposed line scan generated from 20 rows at the bottom of the image.

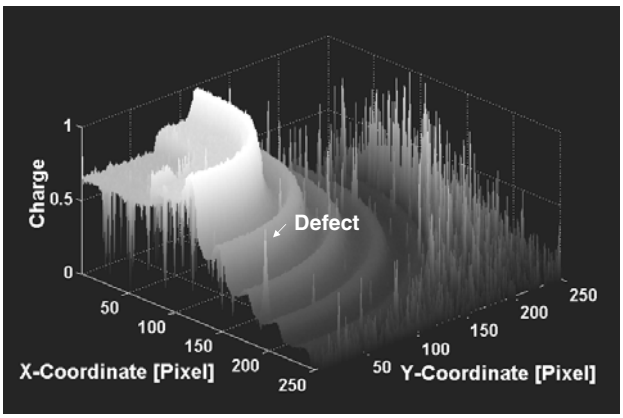

Figure 7. Three-dimensional median value IBIC maps generated using the same data as in figure 5(d).

Peak 'b'—representing the charge collection efficiency of the first field ring—shows a significant increase of the charge collection efficiency when the voltage is increased from 40 to 2290 V. Thus, the spectral information can be used to extract particular features of the electric field distribution of the device.

In figure 6 another area of the diode at a voltage of 1800 V is scanned by the ion beam. The superimposed line scan was generated from the lowest 20 rows of this image and shows pronounced peaks at the p–n junction and the outer edge of the field rings.

Figure 7 shows a three-dimensional plot of the collected charge for a bias voltage of 2290 V, corresponding to the bottom image in figure 5. The increase of the signal at the outer edges is clearly visible. The defect area located between the second and third field rings causes the peak indicated by the white arrow in the three-dimensional plot.

An enlarged median value image of this defect region is shown in figure 8. Decreasing the bias voltage reduces the charge collection efficiency drastically and the defect cannot be

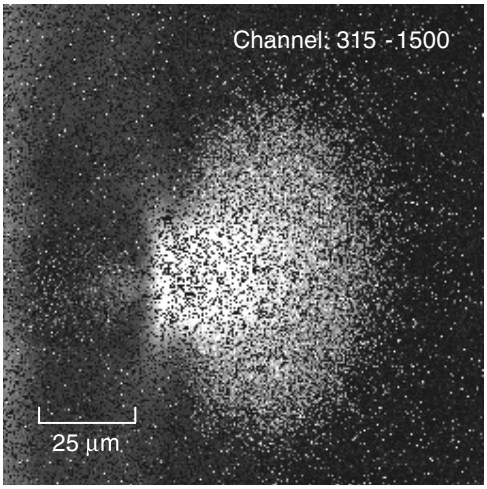

Figure 8. A zoomed image of the defect indicated in figures 5(d) and 7.

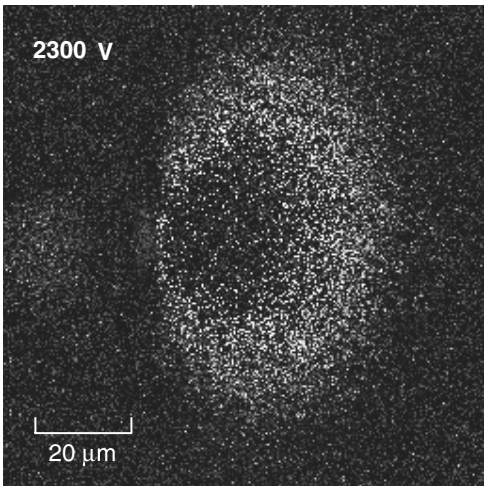

Figure 9. A zoomed image of the defect indicated in figures 5(d) and 7, but at a bias voltage increased by 10 V. The IBIC signals at the centre of the defect appear dark because of an overflow of the data acquisition unit.

identified any longer. Increasing the bias voltage slightly above 2290 V leads to a rapid increase of the multiplication events due to the high electrical field. This is shown in the median value image of figure 9 for a bias voltage of 2300 V. The strong increase of the charge carrier multiplication causes an overflow of the IBIC signals when the ion beam strikes the centre of the defect area. This results in the ring-shaped pattern of the defect.

4. Time differential IBIC microscopy

We consider here the utility of time differential IBIC microscopy applied to large, high voltage devices. As already mentioned, 100% charge collection efficiency can be assumed everywhere in the depletion region, as long as trapping and recombination can be neglected. However, the

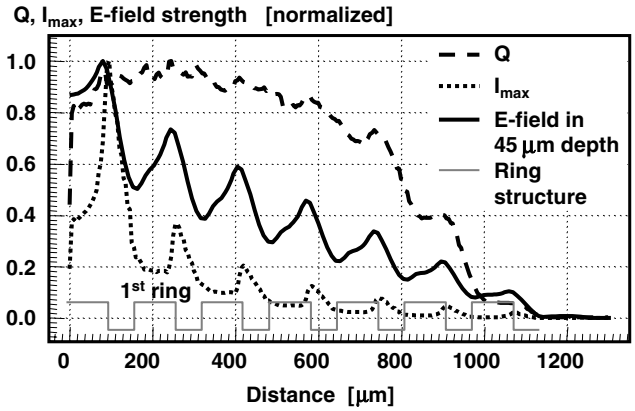

Figure 10. Simulated line scans of the current maxima $I_{\max}$ and the integrated charge Q, calculated both from the simulated IBIC signal and from the electrical field distribution E in a depth of 45 μm (the range of a 2 MeV proton) as a function of the distance. The ring structure is indicated by the thin line at the bottom of the plot.

drift velocity v_{d} depends on the electric field strength E according to $v_{\mathrm{d}} = \mu(E)E$, where μ is the mobility. For large devices (millimetres rather than microns), E-field variations will be reflected in temporal variations in the IBIC pulse. Therefore, the shape of the induced current pulses (characterized by the rise time, amplitude and duration) may vary with the local electric field strength. In the following, we present some simulation results showing how the temporal behaviour of the IBIC pulses is influenced by the local electric field.

5. Simulations

Figure 10 shows the results obtained with the device simulator MEDICI when the diode is biased with a reverse voltage of 1250 V. The field ring structure of the diode is indicated by the broken curve. The electric field distribution E has been calculated for a depth of about 45 μm from the surface, which is comparable to the range of the 2 MeV protons used in the experiments. The electrical field distribution shows peaks at the outer edges of the field rings and the edge of the main p region, which is in good agreement with the experimental results.

Local irradiation with protons was modelled by charge carrier generation in the device as simulated by a TRIM calculation. For the 2 MeV protons used in the experiments, the carrier generation occurs mainly in a depth of about 45 μm. A MEDICI simulation of the current transient produced by a single proton was obtained using the TRIM results and assuming an essentially instantaneous generation process ($t \ll 1$ ns) [8]. By scanning the generation volume (the lateral spacing in the simulation was 5 μm) along the field ring structure—starting at the main diode area and going towards the edge—and plotting $I_{\max}$ versus the distance, we obtain a distribution with a shape very similar to that of the calculated electric field distribution. The charge Q defined as the integral over the current trace depends only weakly on the distance for radial distances smaller than $\approx$400 μm, which is consistent with the assumption of 100% charge collection efficiency.

In figure 11 two IBIC images taken for different ion types and energies are shown for a similar diode. In figure 11(a) a 1 MeV H_2^+ beam has been used applying a bias voltage of about 450 V. Figure 11(b) has been taken using a 2 MeV proton beam. The line scans across the two images have been compared with the simulated line scans (figures 11(c), (d)). The smaller

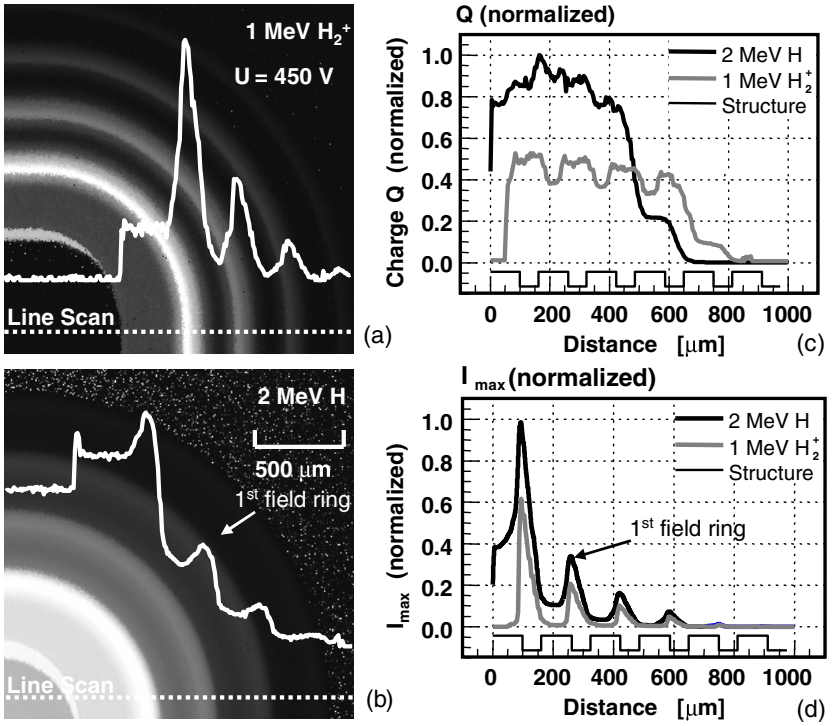

Figure 11. Median value IBIC images taken for different ion types and energies for a similar device. (a) 1 MeV H_2^+ ions, (b) 2 MeV protons. Simulated line scans of the charge (c) and the current maxima (d).

penetration depth of the 1 MeV H_2^+ ions results in ionization closer to the passivation layer. This measurement therefore produces more contrast from the region near the passivation layer at the device surface. Therefore no signal is detectable under the metallization. The peaks at the edge of the main p region and the outer edges from the field rings are very distinctive compared to the line scans for the 2 MeV protons, which have a penetration depth of about 47 μm. This indicates the crucial areas of the structure surface where the electrical field reaches its maximum values.

The simulated charge line scan (figure 11(c)) for the 1 MeV H_2^+ ions shows minima at the field rings. This effect is attributed to charge carrier recombination in non-depleted regions at the surface. The 2 MeV protons generate only a few electron–hole pairs at the device surface. Therefore, the corresponding charge line scan does not show pronounced minima.

Both measured line scans are similar to the corresponding line scan I_{max} (figure 11(d)) constructed from the simulated IBIC signal. In particular, the 1 MeV H_2^+ ions cause distinctive peaks in the experimental as well as in the simulated line scan. It should be noted that the absolute maxima values of the experimental line scans cannot be directly compared to each other, because the 1 MeV H_2^+ ions create fewer electron–hole pairs than the 2 MeV protons.

6. Conclusion and outlook

Finally, we point out that by using a conventional IBIC set-up local maxima of the electrical field distribution within the depletion regions of power devices can be detected and analysed.

Furthermore, our simulation results suggest that the IBIC technique can be further improved by recording and analysing individual IBIC transients. An upgrade of our conventional IBIC set-up for analysing the rise times, durations and amplitudes of the induced current pulses has been completed recently and is now functional.

For the designer of high power devices it is important to consider the transient behaviour of the devices. Therefore, initial experiments evaluating the possibilities of device analyses under transient conditions using IBIC are planned. Separating the transients occurring when a power device is switched for example from the on state to the off state from the IBIC signals is the major challenge in this project.

References

[1] Breese M B H 1996 A review of ion beam induced charge microscopy for integrated circuit analysis *Mater. Sci. Eng.* B **42** 67–76

[2] Yang C, Bettiol A, Jamieson D, Hua X, Phang J C H, Chan D S H, Watt F and Osipowicz T 1999 Investigation of light emitting diodes using nuclear microprobes *Nucl. Instrum. Methods Phys. Res.* B **158** 481–6

[3] Osipowicz T, Sanchez J L, Orlic I, Watt F, Kolachina S, Chan D S H and Phang J C H 1998 Fluence dependence of IBIC collection efficiency of CMOS transistors *Nucl. Instrum. Methods Phys. Res.* B **136–138** 1345–8

[4] Sellin P J, Breese M B H, Knights A P, Alves L C, Sussmann R S and Whitehead A J 2000 Imaging of charge transport in polycrystalline diamond using ion-beam-induced charge microscopy *Appl. Phys. Lett.* **77** 913–5

[5] Sheridan D C, Niu G, Merrett J N, Cressler J D and Ellis C 2000 Tin CHIN-CHE, design and fabrication of planar guard ring termination for high-voltage SiC diodes *Solid-State Electron.* **44** 1367–72

[6] Zmeck M, Osipowicz T, Watt F, Niedernostheide F J, Schulze H J, Fiege G B M and Balk L J 2000 Analysis of high-power devices using proton beam induced currents *Microelectr. Reliab.* **40** 1413–8

[7] Zmeck M, Phang J C H, Bettiol A, Osipowicz T, Watt F, Balk L J, Niedernostheide F-J, Schulze H J, Falck E and Barthelmess R 2001 Analysis of high power devices using proton beam induced charge microscopy *Microelectr. Reliab.* **41** 1519–24

[8] Knoll G F 1999 *Radiation Detection and Measurement* (New York: Wiley)

[9] Breese M B H, Jamieson D N and King P J C 1996 Ion beam induced charge microscopy *Materials Analysis Using a Nuclear Microprobe* (New York: Wiley)